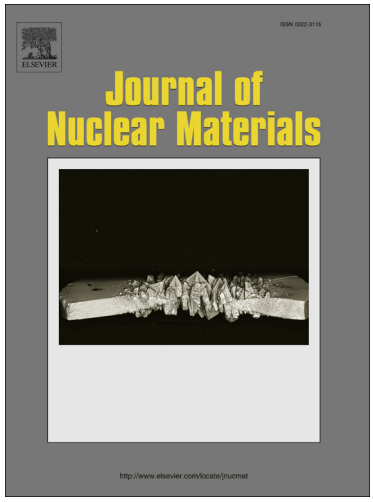

Thermodynamic Evaluation of the Np-Zr System Using CALPHAD and Ab Initio methods

Wei Xiong, Wei Xie, Dane Morgan

PII: S0022-3115(14)00380-8
DOI: http://dx.doi.org/10.1016/j.jnucmat.2014.06.023
Reference: NUMA 48228

To appear in: *Journal of Nuclear Materials*

Received Date: 16 September 2013
Accepted Date: 12 June 2014

Please cite this article as: W. Xiong, W. Xie, D. Morgan, Thermodynamic Evaluation of the Np-Zr System Using CALPHAD and Ab Initio methods, *Journal of Nuclear Materials* (2014), doi: http://dx.doi.org/10.1016/j.jnucmat.2014.06.023

Thermodynamic Evaluation of the Np-Zr System Using CALPHAD and Ab Initio methods

Wei Xiong [1,*], Wei Xie [2], Dane Morgan [1,2,3,*]

1. Department of Materials Science and Engineering, University of Wisconsin-Madison, Wisconsin 53706, USA

2. Materials Science Program, University of Wisconsin-Madison, Wisconsin 53706, USA

3. Department of Engineering Physics, University of Wisconsin-Madison, Wisconsin 53706, USA

* Corresponding authors:

Email: wxiong@yahoo.com (W. Xiong), ddmorgan@wisc.edu (D. Morgan)

Address: 1509 Engineering Drive, Madison, WI 53706, USA

Tel./Fax: +1 608 265 5879

Abstract

A new thermodynamic description of Np-Zr alloys is developed using the CALPHAD (CALculation of PHAse Diagrams) method based on available experimental information on phase equilibria and select ab initio energetics. The present thermodynamic description shows improvements compared to previous models in the predicted phase diagram when comparing to assessed reliable experimental data. Ab initio density functional theory (DFT) calculations are also performed on all known stable solid phases of Np-Zr alloys and the end member Np and Zr metals. Comparing to the formation energetics predicted from the CALPHAD models of both this work and the previous study we find that DFT with the generalized gradient approximation (GGA) to the exchange-correlation potential overestimates the formation enthalpies of Np and Np-Zr by about 0.15 eV/atom, and the so-called DFT+U approach with a U_{eff} of near 0.65 eV can reduce this error by about 0.07-0.10 eV. Our comprehensive comparision between existing CALPHAD, ab initio and experimental results for Np-Zr indicates a need for further experiments on the phase equilibrium.

1. Introduction

Np-Zr is an important alloy system for nuclear fuels due to its potential uses in multiple applications. For example, Np-Zr-H can be used in the hydride fuel as an integral fuel-moderator system, since the concentration of hydrogen in the hydride is comparable to that of hydrogen in

liquid water of LWR cores [1]. In addition, the Np-Zr-H alloys are also considered as the actinide hydride targets in fast reactors, which were proposed to reduce the actinide content in nuclear waste [2]. Furthermore, Np-Zr is a binary component of the U-Pu-Zr-MA (MA = Minor Actinides Np, Am, Cm) alloy, which is a promising metallic fuel for fast nuclear reactors [1]. Recent research activities on phase equilibria of the U-Pu-Zr-MA systems [3-6] have contributed to understanding of the phase behavior of the actinide alloys for desiging new actinide materials.

Because of the importance of the Np-Zr system in nuclear engineering applications, it is necessary to study thermodynamics of the Np-Zr alloys, and to provide a reasonable thermodynamic description of this system for constructing reliable actinide thermodynamic databases.

Up to now, thermodynamic modeling of the Np-Zr system has been performed by two research groups [7, 8]. However, the optimized Np-Zr phase diagrams in the two studies [7, 8] still leave some uncertainty unresolved, which motivates further thermodynamic modeling of this system. One aim of this work is to develop a CALPHAD model of the Np-Zr system, which can be utilized for the thermodynamic modeling of multi-component actinide systems in the future. Moreover, it has recently been found that the DFT+U method can provide useful energetic calculations of the U-Zr alloys [9, 10] for phase diagram development. Therefore, it is interesting to see if DFT+U calculations can also be applied to the Np-Zr system to assist in the thermodynamic modeling.

2. Literature Review

2.1. Experimental data on Np-Zr phase diagrams

All of the experimental information on Np-Zr of which we are aware that can be used in thermodynamic modeling is summarized in Fig. 1(a). Firstly, a major source of experimental phase equilibria data was from the research group of Gibson et al. [11, 12], who provided the invariant equilibria temperatures of the Np-Zr phase diagram using both in-situ and ex-situ Differential Thermal Analysis (DTA) measurements [11, 12]. Using the so-called in-situ DTA measurement invented by Gibson et al. [11, 12], pure elemental Np and Zr were placed together in a Ta or Al_2O_3 crucible and the Np-Zr alloying proceeded upon fusion of Np. However, since the melting temperature of pure Zr is higher than the maximum operating temperature (1200 ºC), it is hard to confirm that an equilibrium alloy was achieved during the in-situ DTA measurement, which was why some ex-situ (regular) DTA were also performed using arc-melted alloys. As shown in Fig. 1(a), the differences between in-situ and ex-situ are relatively small. Therefore, it

is reasonable to set a relatively high weight during the optimization on the reported temperatures of the invariant reaction of the Np-Zr system. However, it should be noted that the invariant reaction type and the phases involved were not determined completely in the study by Gibson et al. [11, 12]. Later Rodriguez et al. [13] also studied this binary experimentally. As shown in Fig. 1, they determined the tie-line by electron microprobe analysis (EMPA), measured some phase transition temperatures through dilatometry, and studied the microstructures of several phase regions using metallography. However, their tie-line construction is suggested to be inaccurate on the Np-rich corner (for example, see tie-lines for (γNp)+(βZr) and (γNp)+δ at 793 and 868 K in Fig. 1(c)), since we found it is hard to fit their values consistently with other experimental data during the thermodynamic optimization. The possible reasons for the tie-line issues are uncertain, as the details of their EPMA measurement methodology were not reported [13]. Rodriguez et al. [13] also used dashed lines to sketch the constructed phase boundaries, which usually means large uncertainties in the measurements. In addition, Rodriguez et al. [13] indicated that the bcc solution phases (γNp) and (βZr) have continuous mutual solubility in the whole composition range, which is not supported by later experiments [14]. As a consequence, in this work, the EMPA results from Rodriguez et al. [13] were assigned with a relatively low weight in the thermodynamic optimization. Finally, a third experiment by Okamoto et al. [14] performed X-ray diffraction on (γNp) and (βZr) up to 973 K, which provided direct evidence for a lack of continuous mutual solubilty between the two phases. Okamoto et al. [14] also estimated the decomposition temperature of the δ phase to be around 823 K.

Despite the above mentioned studies, the phase diagram and phase equillibria of the Np-Zr system are still not well established. For example, except for the reaction temperature, the invariant reaction type has not been fully determined. Also, as summarized in Fig. 1, experimental data of the solubility of Zr in Np allotropes are also mostly lacking. Moreover, although there are some efforts measuring the temperatures of phase transitions involving the θ phase, the crystalline structure of the θ phase is still undetermined, and thus so far it can only be considered as a stoichiometric phase in the CALPHAD modeling. Besides phase diagram data, to the best of our knowledge, there is also no available direct measurement of the thermodynamic properties of the Np-Zr alloys. Therefore, we hope that by integrating ab initio calculations and CALPHAD modeling in this work we can provide some reasonable prediction of the thermodynamic properties of this binary alloy, such as the enthalpy of formation of the solid phases.

2.2. Reported ab initio calculations and thermodynamic modeling of Np-Zr

So far there are two CALPHAD models available for the Np-Zr system [7, 8]. The first is performed by Kurata [7], which we did not reproduce and compare our results to in this work because 1) the thermodynamic parameters of the δ phase is not provided in Ref. [7], and 2) the calculated phase diagram shown in Ref. [7] shows complete mutual solubility between (γNp) and (βZr), which is not consistent with the commonly accepted experimental observation [14] discussed in Section 2.1.

A second study is reported by Bajaj et al. [8]. They performed ab initio calculations using the KKR-ASA-CPA model (KKR: Korringa-Kohn-Rostoker, ASA: Atomic Sphere Approximation, CPA: Coherent Potential Approximation) to explore the mutual solubility of the bcc (γNp, βZr) structure,. Their calculated enthalpies of formation for (γNp, βZr) referencing to pure bcc γNp and βZr are positive at 0 K over the whole composition range, which is consistent with Okamoto et al.'s experimental results [14]. However, it seems that the phase diagram calculated by Bajaj et al. [8] using CALPHAD did not catpture well some features of the assessed reliable experimental data shown in **Fig. 1**, as we will discuss in detail in Section 5.

3. Thermodynamic models used in the CALPHAD modeling

Thermodynamic models used in this work for the stable phases in the Np-Zr system are summarized in **Table 1.**

3.1. Solution phase

There are six solution phases in the Np-Zr system: (αZr) with hcp structure, (βZr) and (γNp) with bcc structure, (αNp) with orthorhombic_AC structure, and (βNp) with tetragonal_AD structure.

These solution phases can be modeled with the substitutional solution model by the following equation:

$$G_{\mathrm{m}}^{\phi} = x_{\mathrm{Np}}\,{}^{\mathrm{o}}G_{\mathrm{Np}}^{\phi} + x_{\mathrm{Zr}}\,{}^{\mathrm{o}}G_{\mathrm{Zr}}^{\phi} + RT\left(x_{\mathrm{Np}}\ln x_{\mathrm{Np}} + x_{\mathrm{Zr}}\ln x_{\mathrm{Zr}}\right) + {}^{\mathrm{ex}}G_{\mathrm{m}}^{\phi} \qquad (0)$$

where x_{Np} and x_{Zr} are the mole fraction of Np and Zr, respectively. Note that different from Bajaj's work, we only considered αZr with hcp structure as the ground state phase of Zr metal, and the reason is discussed in detail in Section 5.1 below.

3.2. Intermetallic compounds

There are two intermetallic phases in the Np-Zr system: θ and δ. The crystal structure of the θ(Np,Zr) phase remains undetermined although there has been a suggestion [14] that it is isomorphic with θ(Pu,Zr), whose crystal structure is also only partially known [15]. Consequently, the θ phase is modeled as a stoichiometric phase in this work. On the other hand, the crystal structure of the δ phase was determined [16] to be a C32 structure with prototype AlB_2, which is the same to the δ phase in the U-Zr system, both isomorphic with the ω phase of pure Zr [17]. As illustrated in **Fig. 2**, the C32 structure has two distinct Wyckoff sites—site I (i.e., the corners of the lattice box) has Wyckoff symbol 1*a* and fractional coordinate (0, 0, 0), while site II (i.e., the two internal positions in the lattice box) has Wyckoff symobol 2*d* and fractional coordinates (1/3, 2/3, 1/2) and (1/3, 2/3, 1/2). Ref. [16] determined that for the δ phase of Np-Zr, site I is occupied only by Zr but site II is occupied by both Np and Zr with an occupancy of 50 to 67 at.% Zr.

Thermodynamic models of both θ and δ phases are described using the sublattice model according to the work by Sundman and Ågren [18, 19]. For instance, the Gibbs energy expression of δ phase can be expressed as:

$$G_{\mathrm{m}}^{\delta} = y_{\mathrm{Np}}^{\mathrm{II}}\,{}^{o}G_{\mathrm{Zr:Np}}^{\delta} + y_{\mathrm{Zr}}^{\mathrm{II}}\,{}^{o}G_{\mathrm{Zr:Zr}}^{\delta} + 2/3\,RT(y_{\mathrm{Np}}^{\mathrm{II}}\ln y_{\mathrm{Np}}^{\mathrm{II}} + y_{\mathrm{Zr}}^{\mathrm{II}}\ln y_{\mathrm{Zr}}^{\mathrm{II}}) + y_{\mathrm{Np}}^{\mathrm{II}}y_{\mathrm{Zr}}^{\mathrm{II}}L_{\mathrm{Zr:Np,Zr}}^{\delta} \qquad (0)$$

where $y_{\mathrm{Np}}^{\mathrm{II}}$ and $y_{\mathrm{Zr}}^{\mathrm{II}}$ are the site fraction of Np and Zr in the second sublattice, respectively; ${}^{o}G_{\mathrm{Zr:Np}}^{\delta}$ and ${}^{o}G_{\mathrm{Zr:Zr}}^{\delta}$ are the Gibbs energies of the two end-members Zr_1Np_2 and Zr_1Zr_2, respectively—both of them of course have the same C32 structure of the δ phase, and the second end member Zr_1Zr_2 is in fact the ω phase of Zr metal; $L_{\mathrm{Zr:Np,Zr}}^{\delta}$ represents the interaction energy term between Np and Zr in the second sublattice in the presence of only Zr in the first sublattice. Note in the subscripts of ${}^{o}G_{\mathrm{Zr:Np}}^{\delta}$, ${}^{o}G_{\mathrm{Zr:Zr}}^{\delta}$ and $L_{\mathrm{Zr:Np,Zr}}^{\delta}$, we use a colon to separate the first and the second sublattice.

4. Ab initio calculations

The stable solid phases of elemental Np and Zr metals and Np-Zr alloys are summarized in **Table 2**. All these phases except the θ phase are calculated in this work. Among them, elemental Np and Zr metal phases, that is, αNp, βNp, γNp, αZr, ωZr and βZr are modeled using their primitive unit cells [17, 20-23]. Np-Zr alloy phases, that is (αNp), (βNp), (αZr), (γNp, βZr), and δ, all have some chemical disorder in the structure. These phases are therefore modeled using supercells that are generated based on their experimental crystal structures [14, 16, 20-22] and the Special Quasi-

random Structure (SQS) method [24] as implemented in the Alloy Theory Automated Toolkit (ATAT) [25]. Firstly, the low and intermediate temperature terminal solution phases (αNp), (βNp) and (αZr) are each studied by one 16-atom supercell with composition 6.3, 6.3 and 93.8 at.%Zr (i.e., containing 1, 1, and 15 Zr atoms), respectively. The solute concentrations have exceeded the experimental solubility limit, but we believe they are acceptable model systems to probe the dilute alloying effect, as the solute atoms are at least 4.6, 5.8, and 7.6 Å apart in these cells, respectively. Secondly, the high temperature solution phases (γNp) and (βZr) both have bcc lattice, although they are not completely miscible, as we discussed above. For the convenience of discussion, we still designate them with a single phase label (γNp, βZr) henceforth. They are studied together by five 16-atom supercells with composition 6.3, 25.0, 50.0, 75.0, 93.8 at.% Zr (i.e., containing 1, 4, 8, 12, and 15 Zr atoms), respectively. Among them, the three structures at 25.0, 50.0, 75.0 at.% Zr are exactly the same to those recommended by Jiang et al. [26]. The other two structures at 6.3 and 93.8 at.% Zr are generated and selected using the same guidelines as used by Jiang et al. [26]. The 16-atom cell has already been found to reach convergence in terms of energy vs. number of atoms for the bcc phase of the testing systems in Ref. [26]. We therefore assume the 16-atom cell is also adequate to represent the disordered bcc phase in the present system of Np-Zr. Finally, the intermediate solution phase δ(Np,Zr)'s crystal structure has been introduced in Section 3 above. Here we calculate two relevant structures of this alloyed phase. The first structure has 50 at.% Zr occupation on site II with the overall chemical formula of $NpZr_2$ (i.e., $Zr_1(Np_{0.5}Zr_{0.5})_2$ in sublattice notation). We find that different from δ(U,Zr) [10], we need 15 atoms to converge the energy and therefore a 15-atom SQS supercell is selected and used in this study. This structure can be considered as a realistic representative of the δ(Np,Zr) phase because its site II occupation is both within the stability range—in fact, it is close to the minimum in the enthalpy of formation curve for δ(Np,Zr) from CALPHAD—and also convenient for constructing SQS cells. The second structure has 0 at.% Zr occupation on site II with the overall chemical formula of Np_2Zr (i.e., Zr_1Np_2 in sublattice notation). Although its occupation on site B is beyond the stability range, it is calculated here because it is one of the two perfectly ordered end members in CALPHAD modeling of δ(Np,Zr) with the sublattice model $(Zr)_1(Np,Zr)_2$ (the other one Zr_1Zr_2 is exactly ωZr, as mentioned above).

All ab initio calculations are performed in the general framework of Density Functional Theory (DFT) [27, 28] using the Vienna Ab initio Simulation Package (VASP) [29, 30]. The electron-ion interaction is described with the projector-augmented-wave (PAW) method [31] as implemented by Kresse and Joubert [32]. The PAW potentials used treat $6s^26p^67s^25f^46d^1$ and $4s^24p^65s^24d^2$ as valence electrons for Np and Zr, respectively. The exchange-correlation

functional parameterized in the Generalized Gradient Approximation (GGA) [33] by Perdew, Burke and Ernzerhof (PBE) [34] is used. The stopping criteria for self-consistent loops used are 0.1 and 1 meV tolerance of total free energy for the electronic and ionic relaxation, respectively. The electronic and ionic optimizations are performed using a Davidson-block algorithm [35] and a Conjugate-gradient algorithm [36], respectively. We do not explicitly set force as a stopping criterion, but when the total free energy is converged according to the criteria above, the Hellmann-Feynman forces on atoms are generally < 0.03 eV/Å for low-symmetry systems, and < 0.001 eV/Å for high-symmetry ones. A cutoff energy of 450 eV is used throughout all calculations. The Brillouin zone is sampled with Monkhorst–Pack k-point meshes [37] given in **Table 2**. We have tested that such k-point meshes and cutoff energy converge the total energy to less than 3 meV/atom, with errors of closer to 1 meV/atom in most cases. The partial occupancies are set using the Methfessel-Paxton method [38] of order one with a smearing width of 0.2 eV. All calculations have included spin polarization.

In a previous study [10], we found that the so-called DFT+U [39, 40] functional with a reasonable Hubbard U parameter can provide some improvement in some calculated ground state properties of U and U-Zr compared to the standard DFT functional when both of them are based on the Generalized Gradient Approximation (GGA) to the exchange-correlation potential as parametrized by PBE[34]. Therefore, we also explore DFT+U for Np and Np-Zr in this study, under the assumption that the valence f-electrons in Np may also contain some level of correlation that can be improved with a DFT+U treatment, as was found for U. Following Ref. [10], we use the DFT+U form suggested by Dudarev et al. [41] which does not introduce explicit local exchange J term but only an effective Hubbard U term that depends on U_{eff}=U-J. This approach also recovers the standard DFT functional exactly when U_{eff} = 0. DFT+U potential is applied only on Np sites in Np metal and Np-Zr alloy, and is not used at all in elemental Zr metal. In comparing the performance of the standard DFT functional with the DFT+U functional, we will refer to the two functionals as DFT and DFT+U, respectively. These names should not be confused with the theories that are usually referred to with the same acronyms. We combat the metastability issue of DFT+U using the U-ramping method [42] with modifications described in Ref. [10].

Regarding the relativistic effects, VASP always includes the mass-velocity and Darwin corrections using methods of Refs. [43, 44] and thus all of our calculations are at least scalar-relativistic. In more accurate calculations, we have included the spin-orbit coupling (SOC) effect in the *LS*-coupling limit. For convenience, in this paper we will designate calculations as SOC and noSOC, respectively for those with and without SOC included. SOC uses quantization axis (0,

0, 1) (i.e., z axis) and starts with the charge density from noSOC and relaxes both the magnitude and direction of the magnetic moments self-consistently. All noSOC calculations treat magnetism collinearly while SOC treats magnetism non-collinearly.

We define the enthalpy of formation for any Np and Np-Zr phase, elemental or alloyed, as $E^{\text{form}}_{\text{Np}_{1-x}\text{Zr}_x} = E^{\text{o}}_{\text{Np}_{1-x}\text{Zr}_x} - (1-x)\,E^{\text{o}}_{\alpha\text{Np}} - xE^{\text{o}}_{\alpha\text{Zr}}$, where $\text{Np}_{1-x}\text{Zr}_x$ is the chemical formula, x is the mole fraction of Zr with $0 \le x \le 1$, and $E^{\text{o}}_{\text{Np}_{1-x}\text{Zr}_x}$, $E^{\text{o}}_{\alpha\text{Np}}$ and $E^{\text{o}}_{\alpha\text{Zr}}$ are the calculated total energy per atom at zero temperature for $\text{Np}_{1-x}\text{Zr}_x$ and the two references αNp and αZr, respectively. Similarly, we define the enthalpy of mixing specifically for the alloyed phase (γNp, βZr) as $E^{\text{mix}}_{\text{Np}_{1-x}\text{Zr}_x} = E^{\text{o}}_{\text{Np}_{1-x}\text{Zr}_x} - (1-x)\,E^{\text{o}}_{\gamma\text{Np}} - xE^{\text{o}}_{\beta\text{Zr}}$, for which γNp and βZr are used as the references. The two enthalpies can be straightforwardly converted to each other using the differences in energies between the two sets of references.

All structural degrees of freedom — volume, ion position, and cell shape — are fully relaxed for all structures in both DFT and DFT+U calculations with and without SOC included, except for those of γNp and (γNp, βZr) which are only volume-relaxed. We find γNp and (γNp, βZr) are mechanically unstable at low temperature, similarly to γU [45, 46] and (γU, βZr) [10]. To mitigate the strong mechanical instability in our zero temperature calculations, we follow the practices of previous calculations [10, 47, 48] to constrain ion positions and lattice shape and perform only volume relaxation for γNp and (γNp, βZr). The atomic radius for Np and Zr is 1.55 and 1.60 Å in Np and Zr metal [49], respectively, differing only by 3%. As a result of this small size mismatch, the cell-internal relaxations that are being excluded are expected to be small, as found in Ref. [10] for U and U-Zr.

5. Results and discussion

The PARROT module in the Thermo-Calc software package version 3.0 was employed for the current thermodynamic optimization[50]. Reliable experimental data discussed in Section 2 were adopted during the thermodynamic modeling. Since bcc is the phase shown in most of the invariant reactions, the preliminary optimization steps focused on adjusting the invariant reactions with the bcc phase involved. The liquid phase was optimized as the second step, and the thermodynamic parameters of the intermetallic compounds were adjusted in the PARROT module as the final step.

Table 1 lists the evaluated thermodynamic parameters of our CALPHAD model. We emphasize that the optimization of these parameters in this work is done primarily by fitting to experimental

phase diagram data. The only three ab initio energetic inputs used in the optimization of the CALPHAD model are ${}^{o}G_{Zr}^{(\alpha Np)}$,, ${}^{o}G_{Zr}^{(\beta Np)}$, and ${}^{o}G_{Np}^{(\alpha Zr)}$, which are the lattice stabilities of pure Zr with the structures of αNp (orthorhombic_AC) and βNp (Tetragonal_AD), as well as that of pure Np with the structure of αZr (Hcp_A3), respectively. These three values are not available in the standard CALPHAD database, and are here roughly estimated by 0 K energies from DFT calculations for ${}^{o}G_{Zr}^{(\alpha Np)}$ and ${}^{o}G_{Zr}^{(\beta Np)}$ and from DFT+U (U_{eff}=0.65 eV) calclations for ${}^{o}G_{Np}^{(\alpha Zr)}$, as listed in **Table 1.** Excepting the above three values, no other ab initio energetics, especially the enthalpy of mixing for (γNp, βZr), are used in the CALPHAD model fitting. They are only used as references to cross-validate with CALPHAD models *a posteriori*.

5.1. Low temperature stability of pure Zr

The previous work by Bajaj et al. [8] developed two CALPHAD models by considering αZr (hcp_A3) and ωZr (Hexagonal_C32) as the ground state of Zr metal, respectively (refered to as Model 1 and Model 2, respectively in Ref.[8] and in our discussion below). Bajaj et al. explained in Ref. [8] that the reason was because their ab initio calculations found αZr's energy to be about 1 kJ/mole higher than ωZr. However, it is more commonly accepted in the literature[51, 52] that αZr is the ground state phase of Zr metal. Facing the discrepancy, we also performed ab initio calculations of pure Zr metal.

Fig. 3 shows the total energy as a function of volume we calculated for all the three stable solid phases of Zr metal─ αZr (hcp_A3), ωZr (Hexagonal_C32) and βZr (bcc_A2). We see that at the equilibrium volumes (i.e., zero pressure), the total energy is in the order αZr < ωZr < βZr. This shows that our DFT-PAW calculations correctly reproduce the better accepted experimental finding [51, 52] that αZr is the most stable ground state phase at zero temperature and pressure, with total energy 96.485 J/mole lower than ωZr. This result also matches those of some recent ab initio calculations using both FPLMTO [48] and PAW [53]. To explain the difference between our and Bajaj et al. [8]'s ab initio results for Zr metal, we point out that one possible reason may be due to structure relaxation. Although Bajaj et al. [8] did not describe the details of their structural relaxation, our earlier calculations performing only one-step automatic full structure relaxation also obtained αZr to be less stable than ωZr. It is only our later calculations manually performing a series of constant volume relaxation to most accurately identify the equilibrium volume and energy that reproduced the correct phase stability reported here.

As a consequence, only the hcp_A3 structure (αZr) as the ground state is optimized in this work. Furthermore, comparisons will be made only to Model 1 of Ref. [8] that considered hcp_A3 (αZr) as the stable Zr phase.

5.2. Comparison of calculated phase diagrams and experimental data

As discussed in Section 2.1 above, the transition temperatures of invariant reations in the Np-Zr system have been well determined in the experiments by Gibson and Haire [11, 12] using both in-situ and ex-situ DTA measurements and should be considered as the most reliable experimental data so far that CALHPAD model of Np-Zr should reproduce. As shown in **Fig. 1 (a) and (c)**, our present CALPHAD model reproduced these transition temperatures rather well. As a first example, our model predicted the two transition temperatures of 823.1 and 910 K that are in excellent agreement with the empty circle (in-situ) and triangle (ex-situ) DTA experimental data points of Gibson and Haire [11, 12] in Fig. 1 (c). In comparison, we note in Fig. 1 (d) that Bajaj et al. [8]'s Model 1 predicted the corresponding two temperatures to be 882 and 852.3 K respectively, which are are about 30 K away from the experimental DTA data points. Another example of how our CALPHAD reproduces well the invariant reaction data can be seen by comparing the difference in the temperatures for the two invariant reactions, (γNp) + (βZr) = δ and (βZr) = δ + (αZr). Our model predicts the two reation temperatures to be 846.4 and 823.1, respectively, differing by 23.3 K. In addition to the excellent agreement for the second temperature 823.1 K that we have already discussed above, the first temperature 846.4 K is also in excellent agreement with the Dilatometry data point of Rodriguez marked by an open cross. We note that Bajaj et al. [8]'s Model 1 predicted this difference to be only 0.03 K (852.33 vs. 852.30 K), which seems to be very small considering the measured values and that thermal analysis has a typical measurement uncertainty as high as 0.1 K. Another improvement in the present model compared to Bajaj et al. [8]'s Model 1 is that our model predicted solubility boundaries of (βZr) that did not show the unusual curvature that Bajaj et al. [8]'s Model 1 predicted between 900 and 1200 K. This type of curvature, while not necessarily incorrect, does seem very uncommon in binary alloy phase diagrams. Overall, the above comparisons between experimental data and the calculated phase diagrams of this work and Ref. [8] indicate that the thermodynamic model in this work may have provided an improved thermodynamic description of the Np-Zr system.

5.3. Calculation of thermodynamic properties

5.3.1. Ab initio energetic calculations of the elemental Np and terminal solution phases

Now we validate ab initio approaches (i.e., DFT vs. DFT+U; noSOC vs. SOC) in modeling the correlation and relativistic effects in Np and Np-Zr. To avoid any bias, we compare ab inito energetics to the predictions from both the CALPHAD model of this work as well as CALPHAD Model 1 of Bajaj et al. [8]. We will see that the conclusion to be reached below is unaffected by which CALPHAD model we compare to.

First, we focus the comparison on all the three known stable solid phases of Np metal as well as the low and intermediate temperature terminal solution phases of Np-Zr alloy in **Figs. 4 and 5,** respectively. The remaining two phases δ(Np,Zr) and (γNp, βZr) are subject to uncertainty due to the controversy on αZr vs. ωZr as ground state phase and the constrained relaxation approach employed to mitigate the mechanical instability, respectively, and we will discuss them separately later. **Figures 4 and 5** show that, similar to U and U-Zr [10], Np and Np-Zr's energetics are significantly overestimated by DFT (i.e., at U_{eff}= 0 eV). This overestimation can be seen by comparing the DFT values to the experimental cohesive energy of αNp [49], the SGTE data for pure elements [54], and the enthalpies predicted by the two CALPHAD models. On the other hand, DFT+U gives smaller formation energies and thus better agreement with the above references. The energetics also evolve as functions of U_{eff} in three stages, similar to those for U and U-Zr [10]. The first stage is between 0 to 1 eV, the second 1 to 2 eV, and the third > 2 eV. The ab initio curves in general cross the experimental or CALPHD reference values at U_{eff} between 0.65 to 0.9 eV.

Figure 6 summarizes the comparison in **Figs. 4 and 5** and shows the root mean square (RMS) of enthalpy differences between ab initio and measured or CALPHAD modeled energetics. At this level of comparison there is no visible difference in the RMS values calculated referencing to the CALPHAD model of this work and to CALPHAD Model 1 of Bajaj et al. [8]. Note that we include only formation energies relative to the end members in Fig. 6. The overall cohesive energy of the stable end members αNp is not considered here as it does not impact phase stability being modeled here. However, the trend in calculated cohesive energy with U_{eff} for αNp is similar to those found for the formation energies of other phases, with an optimal U_{eff} of around 0.6 eV. as shown in Fig. 4 (a). Overall, **Figure 6** shows two qualitative features that are the most important: (1) the RMS of enthalpy differences for the SOC case keeps going down from 0 to 0.9 eV, reaches minimum at 0.9 eV, and gradually increases thereafter; (2) the RMS of enthalpy

differences from SOC calculations are clearly smaller than that of noSOC. Quantitatively, the average RMS of differences is 0.151, 0.076 and 0.029 eV/atom when SOC is included, and 0.166, 0.116 and 0.058 eV/atom when SOC is not included at U_{eff} = 0, 0.65 and 0.9 eV, respectively. These statistics show that (1) DFT yields RMS errors in the enthalpies of about 0.15 eV/atom (these errors are typically due to overestimating the formation energies compared to experimentally derived values), and DFT+U can reduce the error by roughly 0.07-0.1 eV/atom when using an U_{eff} of around 0.65-0.9 eV; (2) Adding SOC will typically lower the RMS error in enthalpy by about 0.03 eV/atom. These results suggest that the modeling of Np and Np-Zr seems to be improved by the use of DFT+U and by adding SOC, which is consistent with our findings on U and U-Zr [9]

5.3.2. Enthalpy of formation for the δ and bcc phases

Given the fairly good agreement between DFT+U and CALPHAD energetics for the better established models of phases discussed above in Section 5.3.1, we proceed to discuss the ab initio results for the more controversial phases δ(Np,Zr) and (γNp, βZr), whose energetics are shown in **Figs. 7 and 8**, respectively.

Figure 7 shows the enthalpy of formation for δ(Np,Zr). Firstly we note that our CALPHAD predicted enthalpy is in agreement with that from Bajaj et al.'s model 1 [8] that also considered αZr as the ground state of Zr. The value from Bajaj et al.'s Model 2 that treated ωZr as the ground state is also plotted in Figure 7 for the sake of completeness, but we will not discuss it below. An evident feature is that the CALPHAD curves from both our model and Bajaj et al.'s Model 1 are concave upward, with a minimum near 66.7 at.% Zr. In comparsion, our ab initio curves are also concave upward at $U_{eff} \leq 0.65$ eV but turn into concave downward when $U_{eff} \geq 0.9$ eV. Such result suggests that although U_{eff} = 0.9 eV is the statistical optimal U_{eff} value when only considers enthalpy at a single composition, as shown in **Fig. 6** above, it fails to reproduce the qualitative curvature of the energy curve of δ(Np,Zr) when we consider several compositions. This curvature is essential to reproduce if the energetics are going to predict a stable δ(Np,Zr) phase at approximately the right composition. At the smaller U_{eff} = 0.65 eV, the correct curvature is still reproduced, and in terms of quantitative difference, the ab initio calculated enthalpy is also reasonably close to that of the CALPHAD data near the two ends of the curve although somewhat larger in the middle at 66.7 at.% Zr. It is possible that a minor improvement in agreement between the DFT+U and CALPHAD values may be obtained through exploring additional U_{eff} values between 0.65 and 0.9 eV, but considering the range of intrinsic uncertainty in both CALPHAD and ab initio predictions, further search is probably not too meaningful and thus is

not performed. Overall, for δ(Np,Zr) we find the difference in ab initio and CALPHAD energies are very similar to those found for the better constrained phases discussed in Section 5.3.1, in that DFT also significantly overestimates the energetics for δ(Np,Zr) by about 0.15 eV/atom, and DFT+U reduces the error by about 0.10 eV/atom using U_{eff} near 0.65 eV.

Figure 8 shows the enthalpy of mixing for (γNp, βZr). Again, we also note the difference between the CALPHAD result of this work and Bajaj et al.'s [8], the former being slightly positive (~0.025 eV/atom) while the later quite substantially positive (~0.3 eV/atom). We have shown above that our CALPHAD model gives phase boundary that matches existing experimental data equally or better than Bajaj et al.'s [8], which in some sense may suggest that the present CALPHAD model's values may be more trustworthy.

To further revolve the discrepancy, we compare them to ab initio results. Someone may have the concern that the CALPHAD model in this work was fitted in a way that biased it towards better match with DFT+U results. This concern is not true, at least for the present phase of (γNp, βZr). As we already mentioned above, our CALPHAD model is developed mainly by fitting to experimental phase boundary data with the only ab initio inputs being the energies for pure Zr metal with the crystal structures of αNp and βNp and that for pure Np metal with the crystal structure of αZr. No ab initio input is used in our CALPHAD model for for (γNp, βZr), and hence our CALPHAD and ab initio results can be used to validate each other.

Figure 8 shows that DFT calculations also give large and positive mixing enthalpy, although our DFT-PAW-SQS results are somewhat smaller than Bajaj et al.'s DFT-KKR-CPA result [8], which may be due to the differences between PAW and KKR and between SQS and CPA. However, all the previous comparisons discussed in Sections 5.3.1 and 5.3.2, as well as our previous work on U-Zr [9, 10]have suggested that DFT+U results in smaller energetics than DFT that are expected to be closer to experimental and/or robust CALPHAD results. We find that this is again the case here for (γNp, βZr), because the DFT+U (0.65 eV)-SOC enthalpy curve in **Figure 8** is again very close to our CALPHAD curve. Both of them also show the same asymmetry that the Np-rich end is higher, although such an asymetry is more pronounced in the ab initio data. Such a match between our ab initio and CALPHAD results that are essentially independently obtained validates both the CALPHAD and ab initio values. Therefore, we argue that (γNp, βZr) possibly also has a slightly positive enthalpy, similar to the bcc phase (γU, βZr) in the U-Zr system as found in Ref. [10]. However, due to lack of direct experimental

thermochemical data, the controversy on this high temperature phase cannot be completely resolved at present, and further experimental validation is needed.

Finally, we note that our finding that DFT+U can provide improved energetics for Np metal and Np-Zr alloys is in consistent with the conclusion of another work of Bajaj et al. that assessed DFT+U's on Np metal [55]. Their suggested optimal Hubbard U for Np metal alone is around 2.2 eV, and because they set the exchange J to 1 eV, the optimal U_{eff} is 2.2-1 = 1.2 eV, which is close to our suggested Ueff value of 0.65-0.9 eV for Np and Np-Zr's overall modeling. Bajej et al. pointed that "large changes in volumes supplemented by magnetic transitions" happen when U_{eff} is larger than the optimized U_{eff} region. We note here that similar to what have observed in U and U-Zr system [10], at the empricial optiaml U_{eff} region of 0.65-0.9 eV, volume from DFT+U for Np and Np-Zr is also improved comparing to experimental data and those unphysical expansion is not present. There is indeed some emergence of small magnetic moments, which can be unphysical for at least Np metal, suggesting the DFT+U solution to Np and Np-Zr may not be perfect, but this imperfection does not seem to affect the energetic results that is the focus of our study.

5.3.3. Model predicted excess entropy of mixing for the liquid phase

The comparison of excess entropy of mixing for the liquid phase at 2500 K from this work and Bajaj et al. [8] is shown in **Fig. 9**. The excess entropy of mixing of a metallic liquid is expected to be in the range of −10 to 5 *J*/(*mol·atom·K*) [56-58]. While the model from this work produces excess entropies of mixing in this range the values from Bajaj et al. [8] are outside this range, which possibly is contributing to the improvements in the predicted phase boundary and enthalpy as we discussed before.

6. Conclusions

The thermodynamic description of the Np-Zr system has been re-optimized in CALPHAD modeling. A set of self-consistent thermodynamic parameters have been achieved. These parameters can be employed to describe the known experimental data for the Np-Zr phase diagram, and to predict reasonable thermodynamic properties of the Np-Zr alloys.

Ab initio DFT calculations for Np-Zr are performed and used to provide some information for the CALPHAD modeling and validation of a DFT+U approach for obtaining more accurate energies. For Np metal and Np-Zr alloy, the PBE parametrization of the GGA functional is found to overestimate the formation enthalpies of Np and Np-Zr compounds by about 0.15 eV/atom, and

the so called DFT+U method with a reasonable U_{eff} of near 0.65 eV can reduce this error by about 0.07-0.10 eV. Spin Orbit Coupling (SOC) also lowers the formation enthalpies of Np and Np-Zr by about 0.03 eV/atom. These statistics are quite consistent both when comparing to the CALPHAD model of this work and one from a previous study [8]. These results suggest that use of the DFT+U method with a U_{eff} near 0.65 eV for Np can provide improved energetics for Np-Zr and possibly other alloys of Np and transition metals.

This work provides a CALPHAD model for the Np-Zr systems that shows some improvements in the model predicted phase diagram compared to the previous models. However, a robust and comprehensive thermodynamic understanding of the Np-Zr system will need additional experimental investigation to validate the current modeling results, resolve existing controversies and suggest further improvements.

Acknowledgements

This research was supported by the US Department of Energy's Nuclear Energy University Programs under Contract No. 00088978. Wei Xiong is grateful to the Thermo-Calc software Company, Sweden, for providing the Thermo-Calc software package to perform the thermodynamic modeling. We gratefully acknowledge computing support for this work from Idaho National Laboratory's Center for Advanced Modeling and Simulation. Authors thank Prof. Y. Austin Chang for many contributions to the early stages of the project that led to this work.

References:

[1] B.A. Pudjanto, K. Konashi, M. Kato, T. Terai, M. Yamawaki, Thermodynamic analysis on the Np-Zr-H system, Journal of Nuclear Materials, 344 (2005) 89-93.
[2] B.A. Pudjanto, K. Konashi, T. Terai, M. Yamawaki, Thermodynamic analysis of Np-Zr-H, Am-Zr-H, Pu-Zr-H systems, Journal of Physics and Chemistry of Solids, 66 (2005) 665-670.
[3] C.B. Basak, N. Prabhu, M. Krishnan, On the formation mechanism of UZr2 phase, Intermetallics, 18 (2010) 1707-1712.
[4] K.T. Moore, G. van der Laan, Nature of The 5f States in Actinide Metals, Reviews of Modern Physics, 81 (2009) 235-298.
[5] A.J. Schwartz, H. Cynn, K.J.M. Blobaum, M.A. Wall, K.T. Moore, W.J. Evans, D.L. Farber, J.R. Jeffries, T.B. Massalski, Atomic structure and phase transformations in Pu alloys, Progress in Materials Science, 54 (2009) 909-943.
[6] A.P. Moore, B. Beeler, M. Baskes, M. Okuniewski, C.S. Deo, Atomistic Ordering in Body Centered Cubic Uranium-Zirconium Alloy, MRS Online Proceedings Library, 1514 (2013) 27-35.
[7] M. Kurata, Thermodynamic database on U-Pu-Zr-Np-Am-Fe alloy system II - Evaluation of Np, Am, and Fe containing systems, IOP Conf. Series: Materials Science and Engineering, 9 (2010) 0120231-0120238.

[8] S. Bajaj, A. Garay, A. Landa, P. Soderlind, P. Turchi, R. Arroyave, Thermodynamic study of the Np-Zr system, Journal of Nuclear Materials, 409 (2011) 1-8.
[9] W. Xiong, W. Xie, C. Shen, D. Morgan, Thermodynamic Modeling of the U-Zr System - A Revisit, Journal of Nuclear Materials, 443 (2013) 331-341.
[10] W. Xie, W. Xiong, C.A. Marianetti, D. Morgan, Correlation and relativistic effects in U metal and U-Zr alloy: validation of ab initio approaches, Physical Review B: Condensed Matter and Materials Physics, 88 (2013) 235128.
[11] J.K. Gibson, R.G. Haire, High-temperature DTA of transuranium materials with applicaiton to the Np-Zr phase daigram, Thermochimica Acta, 207 (1992) 65-78.
[12] J.K. Gibson, R.G. Haire, Investigation of the neptunium-zirconium phase daigram by differential thermal analysis, Journal of Nuclear Materials, 201 (1993) 225-230.
[13] R.J. Rodriguez, C. Sari, A.J.C. Portal, Investigation of the Np-Zr and U-Zr-Np systems, Journal of Alloys and Compounds, 209 (1994) 263-268.
[14] Y. Okamoto, R.G. Haire, J.K. Gibson, T. Ogawa, The investigation of selected Np-Zr alloys by X-ray diffraction up to 700 degrees C, Journal of Alloys and Compounds, 232 (1996) 302-306.
[15] A.F. Berndt, Theta Phase in Plutonium-Zirconium System, Journal of the Less-Common Metals, 12 (1967) 82-83.
[16] M.M. Gensini, R.G. Haire, J.K. Gibson, Investigation of the Neptunium-Zirconium System by X-Ray-Diffraction, Journal of Alloys and Compounds, 213 (1994) 402-405.
[17] J.C. Jamieson, Crystal Structures of Titanium, Zirconium, and Hafnium at High Pressures, Science, 140 (1963) 72-73.
[18] B. Sundman, J. Ågren, A regular solution model for phase with several components and sublattices, suitable for computer applications, Journal of Physics and Chemistry in Solids, 42 (1981) 297-301.
[19] M. Hillert, The compound energy formalism, Journal of Alloys and Compounds, 320 (2001) 161-176.
[20] W.H. Zachariasen, Crystal-chemical studies of the 5f series of elements. XVII. The crystal structure of neptunium metal, Acta Crystallographica, 5 (1952) 660-664.
[21] W.H. Zachariasen, Crystal-chemical studies of the 5f series of elements. XVIII. Crystal structure studies of neptunium metal at elevated temperatures, Acta Crystallographica, 5 (1952) 664-667.
[22] J. Goldak, L.T. Lloyd, C.S. Barrett, Lattice Parameters Thermal Expansions and Gruneisen Coefficients of Zirconium 4.2 to 1130 Degrees K, Physical Review, 144 (1966) 478-484.
[23] A. Heiming, W. Petry, J. Trampenau, W. Miekeley, J. Cockcroft, The Temperature-Dependence of the Lattice-Parameters of Pure Bcc Zr and Bcc Zr-2 at-Percent-Co, J. Phys.: Condens. Matter, 4 (1992) 727-733.
[24] A. Zunger, S.H. Wei, L.G. Ferreira, J.E. Bernard, Special Quasirandom Structures, Physical Review Letters, 65 (1990) 353-356.
[25] A. van de Walle, M. Asta, G. Ceder, The Alloy Theoretic Automated Toolkit: A user guide, Calphad-Computer Coupling of Phase Diagrams and Thermochemistry, 26 (2002) 539-553.
[26] C. Jiang, C. Wolverton, J. Sofo, L.Q. Chen, Z.K. Liu, First-principles study of binary bcc alloys using special quasirandom structures, Physical Review B, 69 (2004).
[27] P. Hohenberg, W. Kohn, Inhomogeneous Electron Gas, Physical Review B, 136 (1964) 864-871.
[28] W. Kohn, L.J. Sham, Self-Consistent Equations Including Exchange and Correlation Effects, Physical Review, 140 (1965) 1133-1138.
[29] G. Kresse, J. Furthmuller, Efficient iterative schemes for ab initio total-energy calculations using a plane-wave basis set, Physical Review B, 54 (1996) 11169-11186.
[30] G. Kresse, J. Hafner, Ab initio Moleculear Dynamics for Liquid Metals, Physical Review B, 47 (1993) 558-561.

[31] P.E. Blochl, Projector Augmented-Wave Method, Physical Review B, 50 (1994) 17953-17979.
[32] G. Kresse, D. Joubert, From ultrasoft pseudopotentials to the projector augmented-wave method, Physical Review B, 59 (1999) 1758-1775.
[33] D.C. Langreth, J.P. Perdew, Theory of Nonuniform Electronic Systems .1. Analysis of the Gradient Approximation and a Generalization That Works, Physical Review B, 21 (1980) 5469-5493.
[34] J.P. Perdew, K. Burke, M. Ernzerhof, Generalized gradient approximation made simple, Physical Review Letters, 77 (1996) 3865-3868.
[35] E.R. Davidson, Matrix Eigenvector Methods, in: W.S. G.H.F. Diercksen (Ed.) Methods in Computational Molecular Physics, Bad Windsheim, West Germany, D. Reidel Publishing Company, 1982, pp. 95-113.
[36] M.P. Teter, M.C. Payne, D.C. Allan, Solution of Schrödinger's equation for large systems, Physical Review B, 40 (1989) 12255-12263.
[37] H.J. Monkhorst, J.D. Pack, Special Points for Brillouin-Zone Integrations, Physical Review B, 13 (1976) 5188-5192.
[38] M. Methfessel, A.T. Paxton, High-Precision Sampling for Brillouin-Zone Integration in Metals, Physical Review B, 40 (1989) 3616-3621.
[39] V.I. Anisimov, F. Aryasetiawan, A.I. Lichtenstein, First-principles calculations of the electronic structure and spectra of strongly correlated systems: The LDA+U method, J. Phys.: Condens. Matter, 9 (1997) 767-808.
[40] G. Kotliar, S.Y. Savrasov, K. Haule, V.S. Oudovenko, O. Parcollet, C.A. Marianetti, Electronic structure calculations with dynamical mean-field theory, Reviews of Modern Physics, 78 (2006) 865-951.
[41] S.L. Dudarev, G.A. Botton, S.Y. Savrasov, C.J. Humphreys, A.P. Sutton, Electron-energy-loss spectra and the structural stability of nickel oxide: An LSDA+U study, Physical Review B, 57 (1998) 1505-1509.
[42] B. Meredig, A. Thompson, H.A. Hansen, C. Wolverton, A. van de Walle, Method for locating low-energy solutions within DFT plus U, Physical Review B, 82 (2010) 195128.
[43] L. Kleinman, Relativistic Norm-Conserving Pseudopotential, Physical Review B, 21 (1980) 2630-2631.
[44] A.H. Macdonald, W.E. Pickett, D.D. Koelling, A Linearized Relativistic Augmented-Plane-Wave Method Utilizing Approximate Pure Spin Basis Functions, J Phys C Solid State, 13 (1980) 2675-2683.
[45] P. Soderlind, Theory of the crystal structures of cerium and the light actinides, Advances in Physics, 47 (1998) 959-998.
[46] P. Soderlind, B. Grabowski, L. Yang, A. Landa, T. Bjorkman, P. Souvatzis, O. Eriksson, High-temperature phonon stabilization of gamma-uranium from relativistic first-principles theory, Phys. Rev. B, 85 (2012) 060301.
[47] P. Soderlind, First-principles elastic and structural properties of uranium metal, Physical Review B, 66 (2002) 085113.
[48] A. Landa, P. Soderlind, P.E.A. Turchi, Density-functional study of the U-Zr system, Journal of Alloys and Compounds, 478 (2009) 103-110.
[49] C. Kittel, Introduction to solid state physics, Wiley, Hoboken, NJ, 2005.
[50] B. Sundman, B. Jansson, J.O. Andersson, The Thermo-Calc Databank System, CALPHAD: Computer Coupling of Phase Diagrams and Thermochemistry, 9 (1985) 153-190.
[51] S.K. Sikka, Y.K. Vohra, R. Chidambaram, Omega phase in materials, Progress in Materials Science, 27 (1982) 245-310.
[52] J. Zhang, Y. Zhao, C. Pantea, J. Qian, L.L. Daemen, P.A. Pigg, R.S. Hixson, C.W. Greeff, G.T.G. Iii, Y. Yang, L. Wang, T. Uchida, Experimental constraints on the phase diagram of elemental zirconium, Journal of Physics and Chemistry of Solids, 66 (2005) 1213-1219.

[53] Y.J. Hao, L. Zhang, X.R. Chen, L.C. Cai, Q. Wu, D. Alfe, Ab initio calculations of the thermodynamics and phase diagram of zirconium, Physical Review B, 78 (2008) 134101.
[54] A.T. Dinsdale, SGTE Data for Pure Elements, CALPHAD: Computer Coupling of Phase Diagrams and Thermochemistry, 15 (1991) 317-425.
[55] S. Bajaj, C. Sevik, T. Cagin, A. Garay, P.E.A. Turchi, R. Arroyave, On the limitations of the DFT plus U approach to energetics of actinides, Comp Mater Sci, 59 (2012) 48-56.
[56] H. Okamoto, Reevaluation of thermodynamic models for phase diagram evaluation, Journal of Phase Equilibria, 12 (1991) 623-643.
[57] W. Xiong, Y. Du, X. Lu, J.C. Schuster, H. Chen, Reassessment of the Ce-Ni binary system supported by key experiments and ab initio calculations, Intermetallics, 15 (2007) 1401-1408.
[58] W. Xiong, Y. Kong, Y. Du, Z.K. Liu, M. Selleby, W.H. Sun, Thermodynamic investigation of the galvanizing systems, I: Refinement of the thermodynamic description for the Fe-Zn system, CALPHAD: Computer Coupling of Phase Diagrams and Thermochemistry, 33 (2009) 433-440.

Figure caption:

Figure 1. Comparison of the phase diagram of Np-Zr between the CALPHAD modeling and experimental data [11-13]. (a) calculated phase diagram in this work and experimental data; (b) calculated phase diagram in the work by Bajaj et al. [8] and experimental data [11-13]; (c) magnified part of (a); (d) magnified part of (b).

Figure 2. The Hexagonal_C32 structure of the δ-NpZr phase.

Figure 3. Total energy for Zr metal as a function of volume. noSOC means that spin-orbit coupling effect was not considered in the ab initio calculations, while SOC means the spin-orbit coupling was taken into account.

Figure 4. Ab initio energetics for Np metal at 0 K: (a) cohesive energy for αNp, and enthalpy of formation for (b) βNp and (c) γNp. The data from SGTE and experiments are considered at 298 K. Experimental data in (a) are taken from Ref. [49].

Figure 5. Comparison of the enthalpy of formation for Np-Zr alloy phases at 0 K: (a) (αNp) (6.3 at.% Zr); (b) (βNp) (6.3 at.% Zr); (c) (αZr) (93.8 at.% Zr). The CALPHAD values are calculated at 298 K. The model 1 by Bajaj et al. [8] considering Hcp phase as the stable structure for pure Zr is used for comparison.

Figure 6. RMS of enthalpy differences between ab initio and CALPHAD in this work. βNp, γNp, (αNp) (6.3 at.% Zr), (βNp) (6.3 at.% Zr) and (αZr) (93.8 at.% Zr) are considered. The lines connecting the ab initio results are used for guiding the eyes.

Figure 7. Comparison of the enthalpy of formation of the δ phase between ab initio calculations and CALPHAD modeling. The dotted lines connecting the ab initio results are used for guiding the eyes. Model 1 in the work by Bajaj et al. [8] takes hcp as the stable structure for pure Zr, while model 2 takes the ω phase. (a) Is the case for ab initio calculations with noSOC and (b) is the case for ab initio calculations with SOC.

Figure 8. Comparison of the enthalpy of mixing of the bcc structure between ab initio calculations and CALPHAD modeling. The dotted lines connecting the ab initio results are used for guiding the eyes. (a) Is the case for ab initio calculations with noSOC and (b) is the case for ab initio calculations with SOC.

Figure 9. Comparison of the excess entropy of mixing of the liquid phase at 2500 K between this work and Bajaj et al. [8].

Table 1. Thermodynamic models and optimized CALPHAD type parameters for different phases of the Np-Zr system in this work

Phase	Model	Thermodynamic parameters (Energy unit: J/mol·atom)
Liquid	(Np,Zr)	${}^{0}L_{\mathrm{Np,Zr}}^{\mathrm{Liquid}} = 1142.97$
		${}^{1}L_{\mathrm{Np,Zr}}^{\mathrm{Liquid}} = 10193.88$
(αNp)	(Np,Zr)	${}^{\mathrm{o}}G_{\mathrm{Zr}}^{(\alpha\mathrm{Np})} = 5804 + {}^{\mathrm{o}}G_{\mathrm{Zr}}^{\mathrm{SER}}$
		${}^{0}L_{\mathrm{Np,Zr}}^{(\alpha\mathrm{Np})} = 52892.37$
(βNp)	(Np,Zr)	${}^{\mathrm{o}}G_{\mathrm{Zr}}^{(\beta\mathrm{Np})} = 5331 + {}^{\mathrm{o}}G_{\mathrm{Zr}}^{\mathrm{SER}}$
		${}^{0}L_{\mathrm{Np,Zr}}^{(\beta\mathrm{Np})} = 23559.89$
(γNp,βZr)	(Np,Zr)	${}^{0}L_{\mathrm{Np,Zr}}^{(\gamma\mathrm{Np},\beta\mathrm{Zr})} = 12335.36 + 3.973 \cdot T$
		${}^{1}L_{\mathrm{Np,Zr}}^{(\gamma\mathrm{Np},\beta\mathrm{Zr})} = 4304.16$
(αZr)	(Np,Zr)	${}^{\mathrm{o}}G_{\mathrm{Np}}^{(\mathrm{aZr})} = 19000 + {}^{\mathrm{o}}G_{\mathrm{Np}}^{\mathrm{SER}}$
		${}^{0}L_{\mathrm{Np,Zr}}^{\beta} = -2109.31$
θ	$(\mathrm{Np})_{0.8}(\mathrm{Zr})_{0.2}$	${}^{\mathrm{o}}G_{\mathrm{Np:Zr}}^{\theta} = -635.02 + 0.8 \cdot {}^{\mathrm{o}}G_{\mathrm{Np}}^{\mathrm{SER}} + 0.2 \cdot {}^{\mathrm{o}}G_{\mathrm{Zr}}^{\mathrm{SER}}$
δ	$(\mathrm{Zr})_{1/3}(\mathrm{Np,Zr})_{2/3}$	${}^{\mathrm{o}}G_{\mathrm{Zr:Zr}}^{\delta} = 527.5 + {}^{\mathrm{o}}G_{\mathrm{Zr}}^{\mathrm{SER}}$
		${}^{\mathrm{o}}G_{\mathrm{Zr:Np}}^{\delta} = 7676.68 - 10.05 \cdot T + 1/3 \cdot {}^{\mathrm{o}}G_{\mathrm{Zr}}^{\mathrm{SER}} + 2/3 \cdot {}^{\mathrm{o}}G_{\mathrm{Np}}^{\mathrm{SER}}$
		${}^{0}L_{\mathrm{Zr:Np,Zr}}^{\delta} = -17744.92 + 32.474 \cdot T$
		${}^{1}L_{\mathrm{Zr:Np,Zr}}^{\delta} = -7535.08 + 9.768 \cdot T$

Table 2. Crystal information on Np and Zr allotropy and their solution phases used in the ab initio modeling of this work

Phase	Structure Name	Space Group	Composition (Zr at.%)	Unit Cell Size (atoms/cell)	SQS used?	**k**-point mesh	Expt. Source
αNp	Orthorhombic_A_c	Pnma	0	8	No	5×5×5	Ref. [20]
(αNp)			6.3	16	Yes	5×5×5	Ref. [16]
βNp	Tetragonal_A_d	P4/nmm	0	4	No	6×6×6	Ref. [21]
(βNp)			3.3	16	Yes	4×4×4	Ref. [14]
γNp	Bcc_A2	$Im\bar{3}m$	0	1	No	17×17×17	Ref. [21]
(γNp, βZr)			6.3 25.0 50.0 75.0 93.8	16	Yes	6×6×6	Ref. [14]
βZr			100	1	No	17×17×17	Ref. [23]
δ	Hexagonal_C32	P6/mmm	33.3	3	No	9×9×13	Ref. [14]
			66.7	15	Yes	6×6×6	
ωZr			100	3	No	9×9×13	Ref. [17]
(αZr)	Hcp_A3	$P6_3/mmc$	93.8	16	Yes	4×4×4	Ref. [16]
αZr			100	2	No	8×8×8	Ref. [22]
θ	Tetragonal (not clear)	P4/ncc	20	80	No	Not calculated	Ref. [14]*

* Ref. [14] suggests it isomorphic with θ(Pu,Zr) whose structure has only been partially solved in Ref.[15].